

Kinematics-Guided Reinforcement Learning for Object-Aware 3D Ego-Pose Estimation

Zhengyi Luo ^{*1} Ryo Hachiuma ^{*2} Ye Yuan ¹ Shun Iwase ¹ Kris M. Kitani ¹

¹ Carnegie Mellon University ² Keio University

zluo2@cs.cmu.edu, ryo-hachiuma@hvrl.ics.keio.ac.jp, {yyuan2, siwase, kkitani}@cs.cmu.edu

Abstract

We propose a method for incorporating object interaction and human body dynamics into the task of 3D ego-pose estimation using a head-mounted camera. We use a kinematics model of the human body to represent the entire range of human motion, and a dynamics model of the body to interact with objects inside a physics simulator. By bringing together object modeling, kinematics modeling, and dynamics modeling in a reinforcement learning (RL) framework, we enable object-aware 3D ego-pose estimation. We devise several representational innovations through the design of the state and action space to incorporate 3D scene context and improve pose estimation quality. We also construct a fine-tuning step to correct the drift and refine the estimated human-object interaction. This is the first work to estimate a physically valid 3D full body interaction sequence with objects (e.g., chairs, boxes, obstacles) from egocentric videos. Experiments with both controlled and in-the-wild settings show that our method can successfully extract an object-conditioned 3D ego-pose sequence that is consistent with the laws of physics.

1. Introduction

From a video captured by a single head-mounted wearable camera (e.g., smartglasses, action camera, body camera), we want to infer the wearer’s 3D pose and interaction with objects in the scene, as shown in Figure 1. This is crucial for applications such as virtual/augmented reality, sports analysis, medical monitoring, etc., where third-person views are often unavailable and high-quality estimates of complex and dynamic human motion are needed. However, this task is challenging since the wearer’s body is often unseen from a first-person view and the body motion needs to be inferred solely based on the visual context captured by the front-facing video. Furthermore, modeling

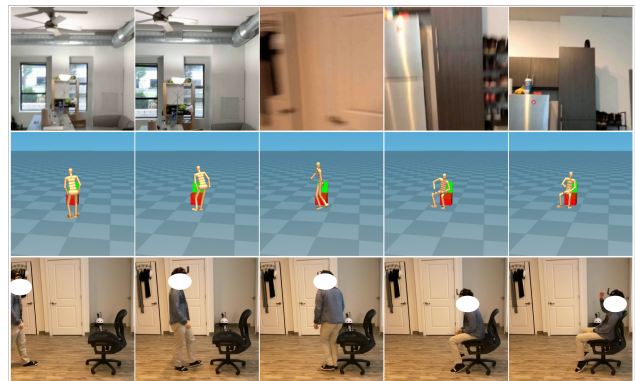


Figure 1: Given an in-the-wild egocentric video, our method can infer physically valid 3D human pose and human-object interaction. **Top:** input egocentric video. **Middle:** estimated 3D human pose and human-object interaction. **Bottom:** reference third person view.

physically realistic human-object interactions requires not only estimating the kinematic motion of the wearer, but also modelling the physical dynamics—the objects need to react to the forces applied by the human action in a physically realistic way. In this paper, we show that it is possible to infer accurate human motion and human-object interaction from a single, forward-facing wearable camera.

First and foremost, we address the important issue of using either 1) kinematics or 2) dynamics-based human pose estimation approaches. 1) Kinematics-based approaches study motion without regard to the forces that cause it. These methods directly output the joint angles of the human model and ignore physics (e.g., how much force is needed at each joint to hold the pose). They can often achieve better pose estimates but produce results that may violate physical constraints (e.g., joints bending the wrong way). Moreover, a kinematics-based model can not faithfully emulate human-object interactions—no physically realistic grasping, pushing, stepping, etc. can be performed without simulating

^{*}indicates equal contribution.

physics. 2) Dynamics-based approaches represent methods that study motions that result from forces. They use a physics simulator and output joint torques to control the humanoid inside the simulator. Thus, these approaches output physically realistic human poses and can lead to convincing human-object interaction (pushing an object will make it move accordingly). However, since no ground truth joint torques are available, dynamics-based approaches are hard to learn and generalize. In this work, we argue that a hybrid approach is needed and propose using the output of the kinematics model as an additional signal to aid the training process and improve the performance of the dynamics model. Instead of training a dynamics model to directly map from the visual context to target joint angles like in prior works [24, 25], we propose to train an additional kinematics pose estimator and employ a novel action representation where the RL policy network is tasked to compute the residual pose against the output from a trained kinematics model. Such a formulation makes use of the accurate pose estimation from a kinematics model while using a dynamics model to refine the estimated pose to obey the laws of physics.

The second key missing piece is the scene context. Prior works [24, 25, 5] have long omitted the semantic scene context from the first-person view due to the complexity of modeling physically correct human-object interactions. However, the presence of objects in the first-person view can often provide a strong prior over the expected human behavior. For example, combining the presence of a chair and the motion of moving forward, turning around, and bending down, we can strongly infer the action of sitting down. Thus, it is imperative for learning models to draw upon this contextual information to make an educated guess about human motion and human-object interaction. To this end, we incorporate the 6-degree-of freedom (DoF) pose of the main object of interest into the state representation of our RL model to make our model aware of the objects' states in the scene.

Another obstacle is the dynamics mismatch between the real world and simulation. As noted by prior work [25], global position and orientation drifts can often be observed over a long horizon of simulation. Such drift can lead to a catastrophic failure of human-object interaction: the humanoid can completely miss the box to push or the chair to sit on. To make sure the correct human-object interaction can be simulated, we propose a fine-tuning step against video evidence to correct the drift in the root trajectories. We use a monocular camera tracking technique, such as Visual Inertial Odometry (VIO) [22, 2], to extract the camera motion and fine-tune our learned policy to match against it. The fine-tuning step alleviates the mismatch between the estimated and real-world global trajectories, leading to a successful human-object interaction.

As there is no public available egocentric video dataset that contains the 3D full-body pose and the 3D object pose, we capture a large-scale motion capture (MoCap) dataset in which the person wears a head-mounted camera and interacts with various objects. We capture three types of interactions: 1) sitting on (and standing up from) a chair, 2) pushing a box, and 3) avoiding obstacles while walking. We also capture an in-the-wild dataset that contains the same set of interactions.

In summary, we tackle the challenging task of extrapolating 3D human motion and human-object interaction from egocentric videos. Our contributions are as follows: (1) We are the first to propose a DeepRL based method for physically valid 3D pose and human-object interaction estimation from egocentric videos. (2) We propose to use a hybrid of kinematics and dynamics approaches and employ a novel action representation in which the dynamics-based model outputs the residual of the action against a learned kinematics-based model. (3) We propose a fine-tuning step to reduce the drift and refine our estimation based on captured video evidence. (4) We experiment with a self-made large-scale MoCap dataset & an in-the-wild dataset, and show that our model outperforms other state-of-the-art methods on several pose-based and physics-based metrics, while generalizing to the in-the-wild settings. Upon visual inspection, our framework can not only recover the 3D human motion from egocentric videos, but also simulate physically correct human-object interactions.

2. Related Works

This section is divided into two parts. First, we will discuss kinematics-based approaches for 3D human pose estimation from egocentric videos. Second, we will discuss recent advancements in dynamics-based humanoid control methods.

2.1. 3D human pose estimation from egocentric videos

The task of estimating the 3D human pose from third-person videos is well researched in the computer vision community [18, 14, 3, 11, 7, 6, 9]. These methods are all kinematics-based and often result in physically invalid motions.

On the other hand, there are only a handful of attempts at estimating 3D full body poses from egocentric videos, due to the ill-posed nature of this task. Most existing methods still assume partial visibility of body parts in the image [21, 17, 23], often through a downward-facing camera. Among works where the human body is mostly not observable, [5, 24, 25, 12], [5] uses a kinematics-based approach where they construct a motion graph from the training motions and recover the pose sequence by solving the optimal pose path. [12] focuses on modeling person-to-

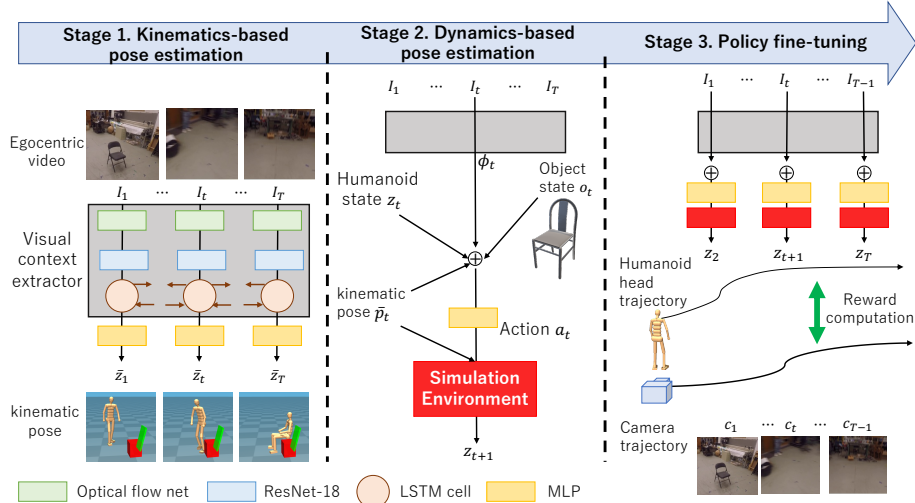


Figure 2: The overview of our proposed pipeline. At first, a pose regressor will estimate the kinematic pose from video evidence. Then an object-aware dynamics-based model will perform and correct the estimated kinematic pose in a physics simulator. Finally, a fine-tuning step corrects the root drifts and produces the final physically valid pose and human-object interaction.

person interactions from egocentric videos and infers the wearer’s kinematic pose conditioning on the other person’s pose. [24, 25, 4], on the other hand, use dynamics-based approaches where a RL-based agent is tasked to perform physically valid human motions. In comparison, our work combines kinematics-based and dynamics-based approaches to achieve both accurate and physically valid pose estimation. In contrast to previous works, we also model human-object interactions such as sitting on a chair and pushing a box on the table. To the best of our knowledge, we are the first approach to estimate the 3D human poses from egocentric video while factoring in human-object interactions.

2.2. Humanoid control for object manipulation

Our work is also connected to controlling humanoids to interact with objects in a physics simulator [15, 16, 1, 10, 26]. The core motivation of this line of work is to learn the necessary dynamics to imitate realistic human motion in a physics simulation.

[1] proposes a hierarchical reinforcement learning approach to generate realistic sitting motion. The authors manually decompose high-level actions (such as sitting) to low-level actions (such as walking, turning, and sitting) from which the proposed meta-controller can stochastically select. They do not aim to estimate the full body pose from egocentric videos, and their motion is limited to sitting. Our approach can not only replicate a diverse set of sitting motions, but also ground sitting motion on video evidence. [10] proposes an approach for enabling humanoid

full-body manipulation and locomotion in simulation. They use a *phased task* in which the task policy is trained to solve different stages of the task and show impressive results in human-object manipulation. Similarly, their generated motion is not grounded on video evidence. [13] uses an action representation in which the target pose is the sum of the kinematic pose and the output of the policy network. Inspired by their work, we also employ this residual action representation to accelerate training and improve stability. Our task is also related to DeepMimic [15] and its video variant [16]. DeepMimic has shown remarkable results in imitating human locomotion skills and is able to combine learned skills to achieve different tasks. However, human-object interaction and video grounding are not considered in their approach.

3. Method

The problem of 3D body pose estimation from egocentric videos can be formulated as follows: from a wearable camera footage $I_{1:T}$, we want to estimate the person’s pose sequence $p_{1:T}$. We propose a three-step method: 1) A kinematic pose regression, 2) object-aware pose correction using dynamics, 3) a fine-tuning step. The overview of our proposed method is depicted in Figure 2.

3.1. Pose Estimation using Kinematics

To recover the kinematic 3D human pose from egocentric videos, we train a regressor that predicts the pose $\bar{p}_{1:T}$ from the input video sequence $I_{1:T}$. Specifically, at first, a

long-short-term-memory (LSTM) based visual context extractor is used to extract visual information from egocentric videos: $I_{1:T} \rightarrow \phi_{1:T}$. Then a multilayer perceptron (MLP) is used to produce the kinematic states from the visual context $\phi_{1:T} \rightarrow \hat{z}_{1:T}$. These states \bar{z}_t consist of the human pose (position on the horizontal plane, orientation of the root, and the joint angles) and velocities (linear and angular velocities of the root and joint velocities). From the kinematic state, we can recover the full kinematic pose sequence $\bar{p}_{1:T}$ that consists of root position, root orientation, and joint angles. We employ mean squared error (MSE) as the loss function to train the regressor: $L(\xi) = \frac{1}{T} \sum_{t=1}^T \|\mathcal{F}(I_{1:T})_t - \hat{z}_t\|^2$, where ξ are the parameters of \mathcal{F} and \hat{z}_t is the ground truth kinematic state from MoCap. In general, this model does not consider the laws of physics like forces or actuation constraints, so the network is easier to train compared to dynamics-based models.

3.2. Object-Aware Pose Estimation using Dynamics

We formulate the task of estimating a physically valid pose sequence $p_{1:T}$ from egocentric RGB images $I_{1:T}$ as a Markov Decision Process (MDP) defined as a tuple $\mathcal{M} = \langle S, A, P, R, \gamma \rangle$ of states, actions, transition dynamics, reward function, and discount factor. The state S and the transition dynamics P are provided by the physics simulator, and the action A and the reward R are computed by the policy π . At each time step t , the agent in state s_t takes an action sampled from the policy $\pi(a_t|s_t)$ while the environment generates the next state s_{t+1} based on that action through physics simulation. Comparing the resulting state of the humanoid with the ground truth, the agent will receive a reward r_t . This process repeats until some termination condition is triggered, such as when the time horizon is reached or the humanoid falls onto the ground. We employ Proximal Policy Optimization (PPO) [19] to calculate the optimal policy π^* that maximizes the expected discounted return $E[\sum_{t=1}^T \gamma^{t-1} r_t]$. At the test time, we roll out the policy π^* to generate a state sequence $s_{1:T}$ from which we extract the output pose sequence $p_{1:T}$.

To enable object-aware motion estimation from egocentric videos that abide by the laws of physics, we innovate on two key points upon prior dynamics-based models: (1) we factor in the object pose into our RL agent’s state representation, (2) we use the result from the pre-trained regressor from the previous step as an additional input to the RL model. Each of the MDP elements is defined as follows:

3.2.1 State.

The state s_t at time step t consists of the humanoid state z_t , the visual context ϕ_t , the kinematic pose state \bar{q}_t , and the object state o_t : $s_t = \langle z_t, \phi_t, o_t, \bar{q}_t \rangle$. z_t consists of the humanoid pose q_t (position and orientation of the root

+ joint angles) and velocity v_t (linear and angular velocities of the root + joint velocity). \bar{q}_t is the output of the kinematic pose regressor \mathcal{F} . Here, we factor in the 6DoF object pose o_t as an additional input to the control policy to enable object-aware 3D pose estimation.

3.2.2 Action.

The action a_t specifies the target joint angles for the proportional-derivative (PD) controller [20] at each degree of freedom (DoF) of the humanoid joints except for the root (Hip). We use a novel residual action representation:

$$q_t^d = \bar{q}_t + \Delta q_t^d, \quad (1)$$

q_t^d is the final PD target, Δq_t^d is the output (action a_t) of the control policy π , and \bar{q}_t denotes the predicted pose of the kinematic pose regressor \mathcal{F} . For joint i , the torque to be applied is computed as $\kappa^i = k_p^i (q_t^d - p_t^i) - k_d^i v_t^i$ where k_p and k_d are manually specified gains. Compared to directly estimating the target joint angle [25], predicting the residual of the target pose against the kinematic pose \bar{q}_t offers a better starting point for the RL policy and results in faster convergence and improved stability.

3.2.3 Policy.

The policy $\pi_\theta(a_t|s_t) = \pi_\theta(a_t|z_t, \phi_t, o_t, \bar{q}_t)$ is represented by a Gaussian distribution with a fixed diagonal covariance matrix Σ . We use a MLP parametrized by θ as our policy network to map the state s_t to the predicted mean μ_t .

3.2.4 Reward function.

The reward function is as follows:

$$r_t = w_p r_p + w_e r_e + w_{rv} r_{rv} + w_{rq} r_{rq} + w_{rp} r_{rp}, \quad (2)$$

where $w_p, w_e, w_{rv}, w_{rq}, w_{rp}$ are the weights of each reward. Our reward is similar to DeepMimic [15], with the exception that we separate the root reward from the pose reward to better motivate the model to match the ground truth root trajectory. More importantly, unlike the conventional object manipulation control methods [15, 10, 16], we do not set any manually designed goal reward for each specific task and only use the pose reward to match ground truth poses to handle multiple interactions. The pose reward r_p measures the difference between the generated pose q_t and the ground truth pose \hat{q}_t in quaternion for each joint on the humanoid except for nonroot joints. The end-effector reward r_e computes the distance between the estimated end-effector (foot, hand, head) position e_t and the ground truth position \hat{e}_t . The root velocity reward r_{rv} penalizes the deviation of the estimated root’s linear l_t and angular ω_t velocity from the ground truth \hat{l}_t & $\hat{\omega}_t$. The ground truth velocity is computed

from the data via finite difference. The root position & orientation rewards r_{rp} & r_{rq} compute the difference between the generated 3D root position p_t & orientation q_t and the ground truth \hat{p}_t & \hat{q}_t in the world coordinate frame:

$$r_p = \exp \left[-5.0 \left(\sum_j \|\bar{q}_t^j \ominus q_t^j\|^2 \right) \right], \quad (3)$$

$$r_e = \exp \left[-4.5 \left(\sum_e \|e_t - \hat{e}_t\|^2 \right) \right], \quad (4)$$

$$r_{rv} = \exp \left[-\|l_t - \hat{l}_t\|^2 - 0.1 \|\omega_t^r - \hat{\omega}_t^r\|^2 \right], \quad (5)$$

$$r_{rq} = \exp \left[-40 \left(\|q_t^r \ominus \hat{q}_t^r\|^2 \right) \right], \quad (6)$$

$$r_{rp} = \exp \left[-45 \left(\|p_t - \hat{p}_t\|^2 \right) \right]. \quad (7)$$

3.2.5 Initial state estimation.

During training, we set the initial humanoid state z_1 and the object state o_1 to the ground truth \hat{z}_1, \hat{o}_1 . At the test time, the starting states of the humanoid and objects are given by the kinematic pose regressor and an off-the-shelf 6DoF object pose estimator, respectively.

3.3. Fine-tuning of the policy network

As mentioned previously, at the test time, the output of the RL model will drift from the ground truth root position and orientation, causing the humanoid to trip and the human-object interaction to fail. Moreover, as the training data cannot cover all object state (position & orientation), it is difficult for the policy to generalize to unseen states.

To overcome this problem, we propose to fine-tune the policy π_θ with test-time video evidence. While capturing the egocentric video, the 6DoF camera motion (position \hat{h}_t^p and orientation \hat{h}_t^q) can be recovered using VIO techniques. Using the camera trajectory as an approximation to head motion, we can fine-tune the trained dynamics-based pose estimator to come up with physically valid pose estimates that conform to the extracted camera trajectory from the video. However, a naive fine-tuning step that only attempts to match humanoid motion with the tracked camera motion may lead to unnatural human poses since the policy may forget how to produce valid human poses. To overcome this issue, we introduce two types of regularization, 1) the fine-tuned pose estimate \bar{p}_t must not deviate from the input kinematics result too drastically. 2) we regularize the action space by penalizing the difference of the output $\tilde{\mu}$ from the pretrained policy network $\tilde{\pi}$ and μ from the fine-tuned policy π . This way, our policy is forced to not deviate too much from its original behavior while trying to conform to the tracked camera trajectory. The overall reward at the

fine-tuning stage is as follows:

$$\hat{r}_t = w_{hp}r_{hp} + w_{hq}r_{hq} + w_{hv}r_{hv} + w_p\lambda_t r_p + w_a(1 - \lambda_t)r_a \quad (8)$$

where $r_{hp}, r_{hq}, r_{hv}, r_p', r_a$ are the rewards for head position, head orientation, head linear and angular velocity, pose, and action, respectively. $w_{hp}, w_{hq}, w_{hv}, w_p, w_a$ are the weighting factors. The head position r_{hp} , orientation r_{hq} , velocity r_{hv} , and rewards are similar to their root counterparts r_{rp}, r_{rq} , and r_{rv} . They are computed similarly and here we use the extracted camera motion as an approximation to ground-truth head trajectory. The pose reward r_p' penalizes the difference of the generated pose p_t and the kinematic pose \bar{p}_t for joints except for the root joint. The action reward penalizes the difference between the mean action of the pretrained policy $\tilde{\mu}$ and the mean action of the current policy μ . Furthermore, we introduce an adaptive weighting factor λ_t on the action reward: if the kinematic regressor \mathcal{F} generates unrealistic poses, the policy should avoid imitating that pose. To this end, we use a confidence value that puts more weight to the kinematic reward if the model has high confidence on the estimated kinematic pose (imitates the estimated kinematic pose more) and leans toward the action reward if the kinematic pose is deemed unrealistic (sticks to the original action more). We calculate this value based on the head linear velocity in local coordinates: where \hat{h}_t^{lv} denotes the linear velocity of the camera and the \hat{h}_t^{lv} denotes the linear velocity of the humanoid head in the local frame, respectively:

$$r_{hp} = \exp \left[-10.0 \left(\|\hat{h}_t^p - h_t^p\|^2 \right) \right], \quad (9)$$

$$r_{hq} = \exp \left[-10.0 \left(\|\hat{h}_t^q \ominus h_t^q\|^2 \right) \right], \quad (10)$$

$$r_{hv} = \exp \left[-0.1 \left(\|\hat{h}_t^v - h_t^v\|^2 \right) \right], \quad (11)$$

$$r_p'(\bar{p}_t, p_t) = \exp \left[-5.0 \left(\sum_j \|\bar{q}_t^j \ominus q_t^j\|^2 \right) \right], \quad (12)$$

$$r_a(\mu, \tilde{\mu}) = \exp \left[-1.0 \left(\|\tilde{\mu} - \mu\|^2 \right) \right], \quad (13)$$

$$\lambda_t = \exp \left[-0.1 \left(\|\hat{h}_t^{lv} - h_t^{lv}\|^2 \right) \right]. \quad (14)$$

4. Experimental Setup

4.1. Dataset

As there is no public dataset available containing the ground-truth full-body human pose and object pose annotations where the person interacts with objects, we record a large-scale egocentric video dataset inside a Mocap studio. It includes three subjects and each subject is asked to wear a head-mounted camera and performs various complex human-object interactions for multiple takes. The actions consist of sitting on (standing up from) a chair, avoiding obstacles, and pushing a box. There are four categories

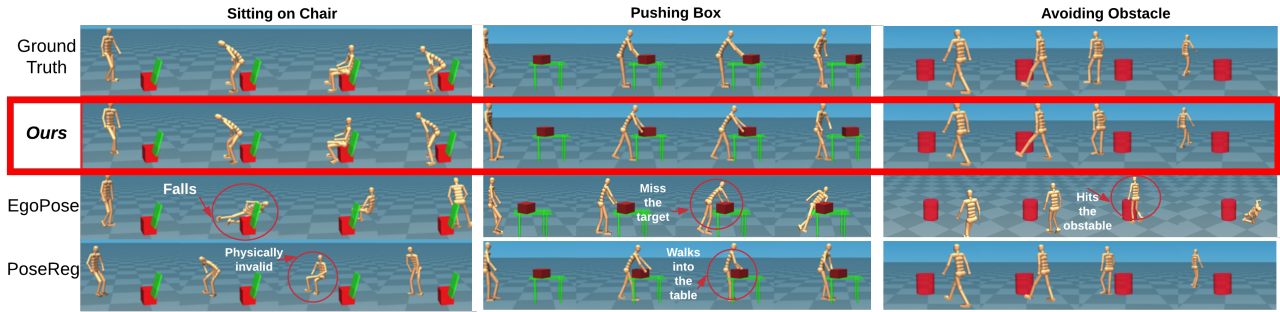


Figure 3: Results of 3D pose and human-object interaction estimation from egocentric videos.

of objects: chairs, tables, boxes, and obstacles. MoCap markers are attached to the camera wearer and the objects to get the 3D full-body human pose and 6DoF object pose. To diversify the ways actions are performed, we ask the actors to vary their performance for each action. We also sample the actors’ initial facing directions and position uniformly from a circle of 3-meter radius. Each take is about six seconds long; 16 to 24 sequences exist for each combination of action and subject. As a result, our MoCap dataset consists of about 250 sequences. We use an 80–20 train test data split on this MoCap dataset. To further showcase the generalization of our method, we also collect an in-the-wild dataset where an additional subject is tasked to perform similar tasks in an everyday setting wearing a head-mounted iPhone. Here, we use Apple’s ARKit to provide camera position & orientation tracking as well as 6 DoF object pose estimation. The in-the-wild dataset has 15 takes in total, each lasting about 6 seconds. For in-the-wild, we use a third-person camera to capture a synchronized side-view of the person and use an off-the-shelf 3D human pose estimator [9] to estimate 3D poses as pseudo-ground truth for evaluation.

4.2. Evaluation metrics

To quantitatively evaluate for 3D pose accuracy and its physical correctness, we employ the following metrics:

Root error (E_{root}): a pose-based metric that measures the difference between the ground truth and the generated root pose, both represented as the 4×4 transformation matrix $M_t(q_t^r | g_t)$ composed of the root orientation q^r and the translation g . The error is calculated using the Frobenius norm: $\frac{1}{T} \sum_{t=1}^T \|I - (M_t \hat{M}_t^{-1})\|_F$ where I is the identity matrix.

Pose Error (E_{joint}): a pose-based metric that measures the difference between the estimated pose sequence $p_{1:T}$ and the ground truth $\hat{y}_{1:T}$, both represented as Euler angles in radians: $\frac{1}{T} \sum_{t=1}^T \|p_t - \hat{p}_t\|_2$. This metric does not consider

the root pose and only compares the body joint angles.

Mean Per Joint Position Error (E_{mpjpe}): a pose-based metric used for our in-the-wild evaluation. As off-the-shelf pose estimator [9] from third-person view uses a different human model [8] than ours, we cannot directly compare the joints’ angles. Thus, we find the common joints (15 in total) between the two human models and directly compare their 3D **positions** in the global coordinate frame. Denote pseudo-ground truth joint position and the estimated joint positions as $J_t, \hat{J}_t \in R^{15 \times 3}$. The metric is calculated as $\frac{1}{T} \sum_{t=1}^T \|J_t - \hat{J}_t\|_2$, measured in millimeters. This metric factors in the root pose as well as the joint angles.

Velocity Error (E_{vel}): a physics-based metric that measures the difference between the estimated joint velocity $v_{1:T}$ and the ground truth $\hat{v}_{1:T}$: $\frac{1}{T} \sum_{t=1}^T \|v_t - \hat{v}_t\|_2$. where v_t and \hat{v}_t are computed by the finite difference. When ground-truth joint angles are available, this metric is calculated as the angular velocity in radians; for in-the-wild evaluation, it is measured in linear velocity in millimeters/second. **Average Acceleration (A_{accel}):** a physics-based metric that uses the average magnitude of joint acceleration to measure the smoothness of the predicted pose sequence, calculated as $\frac{1}{T} \sum_{t=1}^T \|\dot{v}_t\|_1$ where \dot{v}_t denotes the joint acceleration. Similar to the velocity error, for experiments with ground-truth pose available, this metric is calculated in angular acceleration in radians; for in-the-wild evaluation, it is measured in linear acceleration in millimeters/second².

More details about our network and the physics simulator (Mujoco) are provided in the supplementary material.

4.3. Baseline methods

To show the effectiveness of our framework, we compare against two baseline methods: (1) the previous state-of-the-art method in this task, **EgoPose** [25], a dynamics-based approach that produces physically realistic motion but does not factor in object states, and (2) the previous best

kinematics-based approach, also proposed in [25], which we will call **PoseReg**.

5. Results

5.1. Subject-Specific Evaluation.

In this evaluation, we train an individual model for each subject and evaluate on the test split of our MoCap dataset. From the quantitative results in Figure 3, we can see that PoseReg can produce accurate pose estimation, but does not obey the laws of physics (such as sitting in mid-air, walking into the table). EgoPose, on the other hand, often fails to perform the action correctly (falls down or hits the obstacle). Overall, our method (second row) produces 3D human poses closer to the ground truth (top-row) than any other baselines, and successfully performs human-object interaction. **To better visualize the quantitative results, please refer to our supplementary video.**

Table 1 shows the quantitative comparison of our method with the two baseline methods. All results are average across all three subjects. For all actions, we observe that our method outperforms the two baselines across almost all actions and metrics, with occasional worse performance in joint angle estimation with the kinematics-based method (PoseReg). This is expected as PoseReg disregards physics and can estimate poses without constraints, while our method requires estimating a physically valid pose. We find that the humanoid controlled by EgoPose often falls down to the ground and collides with the object, resulting in high pose error. This is expected as EgoPose does not factor in object states into its pose estimation and suffers from error accumulation in global root positions. On the other hand, our object-aware state representation and our fine-tuning step ensure a correct human-object interaction, preventing falls and drifts. We can also observe the low velocity error and acceleration compared to the baseline method, which indicates that our residual action representation produces a more stable and smoother pose estimation.

5.2. Cross-Subject Evaluation.

To further test the robustness, we perform cross-subject experiments where we train our model on two subjects and test on the remaining subject. This is a challenging setting, since people have unique styles and speeds for the same types of interactions. The quantitative results are summarized in Table 2: our method again outperforms other baseline methods in almost all metrics. Especially for the smoothness of the pose (\mathbf{A}_{accel}), our method estimates much smoother (2.0x) pose sequences than those generated from other baseline methods.

5.3. In-the-wild Cross-subject Evaluation.

To demonstrate the generalization of our method to real-world use cases, we further test our method on an in-the-wild dataset. Since there is no ground-truth 3D poses available, we evaluate against pseudo-ground truth 3D pose extracted from a third-person view camera. As shown in Table 3, our method outperforms the baseline methods by a large margin, especially on avoiding and pushing actions where root drifts are prominent. Notice that this dataset is captured in a real-world setting using a different camera (iPhone) than used in the MoCap studio (GoPro), and our method is able to generalize and infer valid human poses and human-object interactions.

5.4. Quantitative Evaluation

As motion is best seen in video, we refer readers to our **supplementary video** for a comprehensive quantitative analysis.

5.5. Ablation Study.

To evaluate the importance of (1) our novel action representation and (2) our fine-tuning step and its reward design, we conduct an ablation study to quantify their benefits. This study is conducted for the first subject’s sitting action. The results of the ablation study are presented in Table 4. To investigate the importance of our action representation (b), we compare the representation employed by [25] (a) in which the policy outputs the target joint of PD control directly (instead of a residual of the kinematics model). The prediction accuracy is improved greatly in all metrics (31%, 48%, 23%, and 31%, respectively) after using our residual action representation.

To investigate the importance of the fine-tuning step and each of its reward terms, we train the comparison models with four types of rewards, (c) head (position, orientation, and velocity) reward, (d) head and kinematic regularization reward, (e) head and action regularization reward, (f) head, and kinematic and action regularization reward. Model (g) has the additional adaptive weighting factor λ_t in addition to the reward (f). From Table 4, without the fine-tuning step, the model performs the worst (b). Our reward (g) outperforms all partial rewards (c-f) in the metrics except for the acceleration metric. Combining each reward term results in the best performance model across all spectrum, showcasing the benefit of our fine-tuning step and its respective rewards.

5.6. Failure cases and limitations

Although our method can produce realistic human pose and human-object interaction estimation from egocentric videos, we are still at the early stage of this challenging task. Our method performs well in the MoCap studio setting and outperforms state-of-the-art methods in-the-wild,

Table 1: *Single-subject* quantitative results for pose-based and physics-based metrics per action

	Sitting				Avoiding				Pushing			
	$E_{root} \downarrow$	$E_{joint} \downarrow$	$E_{vel} \downarrow$	$A_{accel} \downarrow$	$E_{root} \downarrow$	$E_{joint} \downarrow$	$E_{vel} \downarrow$	$A_{accel} \downarrow$	$E_{root} \downarrow$	$E_{joint} \downarrow$	$E_{vel} \downarrow$	$A_{accel} \downarrow$
PoseReg	1.151	0.915	6.431	12.609	0.682	0.638	6.152	12.126	0.909	0.825	6.621	13.058
EgoPose	1.444	1.3445	6.634	10.181	1.293	1.061	7.573	11.945	1.362	1.219	6.704	9.459
Ours	0.607	1.011	5.084	5.489	0.372	0.723	5.889	7.081	0.377	0.820	5.257	5.986

Table 2: *Cross-subject* quantitative results for pose-based and physics-based metrics per action

	Sitting				Avoiding				Pushing			
	$E_{root} \downarrow$	$E_{joint} \downarrow$	$E_{vel} \downarrow$	$A_{accel} \downarrow$	$E_{root} \downarrow$	$E_{joint} \downarrow$	$E_{vel} \downarrow$	$A_{accel} \downarrow$	$E_{root} \downarrow$	$E_{joint} \downarrow$	$E_{vel} \downarrow$	$A_{accel} \downarrow$
PoseReg	1.403	1.775	7.870	11.355	1.326	1.469	7.976	10.768	0.812	1.643	7.260	11.355
EgoPose	1.722	1.887	7.986	13.943	1.514	1.749	9.685	13.942	1.708	1.934	7.870	11.042
Ours	0.756	1.850	6.085	5.880	1.112	1.476	7.368	5.446	0.449	1.631	6.407	5.605

Table 3: *In the wild & Cross-subject* Quantitative results, evaluated against pseudo-ground truth poses from a third person view. Notice that the unit (millimeters) in this table is different from the previous tables where ground-truth annotation is available.

	Sitting			Pushing			Avoiding		
	$E_{mpjpe} \downarrow$	$E_{vel} \downarrow$	$A_{accel} \downarrow$	$E_{mpjpe} \downarrow$	$E_{vel} \downarrow$	$A_{accel} \downarrow$	$E_{mpjpe} \downarrow$	$E_{vel} \downarrow$	$A_{accel} \downarrow$
PoseReg	453.40	26.91	26.48	576.41	23.29	13.55	1680.76	35.49	13.28
Egopose	551.91	28.5	20.47	518.19	26.48	22.73	1540.17	38.25	21.02
Ours	313.76	18.50	4.79	248.85	16.65	4.17	440.08	23.12	5.69

Table 4: Ablation study for the action representation, the fine-tuning step, and fine-tuning reward design.

Action representation	$E_{root} \downarrow$	$E_{joint} \downarrow$	$E_{vel} \downarrow$	$A_{accel} \downarrow$
(a) PD target	1.753	2.049	7.912	12.502
(b) Kinematic residual	1.210	1.064	6.051	8.529

Reward type	$E_{root} \downarrow$	$E_{joint} \downarrow$	$E_{vel} \downarrow$	$A_{accel} \downarrow$
(b) No fine-tuning	1.210	1.064	6.051	8.529
(c) head	0.366	0.920	5.227	6.477
(d) head, kinematic regularization	0.374	0.810	5.090	6.291
(e) head, action regularization.	0.361	0.882	5.136	6.436
(f) head, action + kinematic regularization.	0.340	0.805	5.074	6.351
(g) Full reward (Ours)	0.322	0.788	5.063	6.380

but can still fail to produce natural pose estimation for in-the-wild videos. Due to the severe domain shift, the result of the pose regressor is poor on in-the-wild data and can lead to unnatural motion such as severe foot sliding. As a result, our fine-tuning stage is forced to produce unnatural poses (e.g, long steps, awkward turns) to prevent falling. Furthermore, our method is still limited to a predefined set of interactions where we have data to learn from. To enable pose and human-object interaction estimation for arbitrary actions, much further investigation is needed.

6. Conclusion

In this paper, we tackle, for the first time, physically valid 3D pose estimation from an egocentric video while the person is interacting with objects. We collect a large-scale motion capture dataset to develop and evaluate our method, and extensive experiments have shown that our method outperforms all prior methods. Real-world experiments using an

in-the-wild dataset further show that our method generalizes well to real-world use cases and can infer physically valid 3D human motion and human-object interaction from a front-facing camera feed.

References

- [1] Yu-Wei Chao, Jimei Yang, Weifeng Chen, and Jia Deng. Learning to sit: Synthesizing human-chair interactions via hierarchical control. *ArXiv*, abs/1908.07423, 2019. 3
- [2] J. Engel, J. Sturm, and D. Cremers. Semi-dense visual odometry for a monocular camera. In *IEEE International Conference on Computer Vision (ICCV)*, pages 1449–1456, Los Alamitos, CA, USA, Dec. 2013. IEEE Computer Society. 2
- [3] I. Habibie, W. Xu, D. Mehta, G. Pons-Moll, and C. Theobalt. In the wild human pose estimation using explicit 2d features and intermediate 3d representations. In *IEEE/CVF Conference on Computer Vision and Pattern Recognition (CVPR)*, pages 10897–10906, Jun. 2019. 2
- [4] Mariko Isogawa, Ye Yuan, Matthew O’Toole, and Kris M Kitani. Optical non-line-of-sight physics-based 3d human pose estimation. In *Proceedings of the IEEE/CVF Conference on Computer Vision and Pattern Recognition*, pages 7013–7022, 2020. 3
- [5] Hao Jiang and Kristen Grauman. Seeing invisible poses: Estimating 3d body pose from egocentric video. In *IEEE Conference on Computer Vision and Pattern Recognition (CVPR)*, pages 3501–3509, Jun. 2016. 2
- [6] Muhammed Kocabas, Nikos Athanasiou, and Michael J. Black. Vibe: Video inference for human body pose and shape estimation. *2020 IEEE/CVF Conference on Computer Vision and Pattern Recognition (CVPR)*, pages 5252–5262, 2020. 2

- [7] Nikos Kolotouros, Georgios Pavlakos, Michael J. Black, and Kostas Daniilidis. Learning to reconstruct 3d human pose and shape via model-fitting in the loop. *2019 IEEE/CVF International Conference on Computer Vision (ICCV)*, pages 2252–2261, 2019. 2
- [8] M. Loper, Naureen Mahmood, J. Romero, Gerard Pons-Moll, and Michael J. Black. Smpl: a skinned multi-person linear model. *ACM Trans. Graph.*, 34:248:1–248:16, 2015. 6
- [9] Zhengyi Luo, S. Golestaneh, and Kris M. Kitani. 3d human motion estimation via motion compression and refinement. *ArXiv*, abs/2008.03789, 2020. 2, 6
- [10] Josh Merel, Saran Tunyasuvunakool, Arun Ahuja, Yuval Tassa, Leonard Hasenclever, Vu Pham, Tom Erez, Greg Wayne, and Nicolas Heess. Reusable neural skill embeddings for vision-guided whole body movement and object manipulation. 2019. 3, 4
- [11] Gyeongsik Moon, Juyong Chang, and Kyoung Mu Lee. Camera distance-aware top-down approach for 3d multi-person pose estimation from a single rgb image. In *IEEE Conference on International Conference on Computer Vision (ICCV)*, pages 10113–10142, Oct. 2019. 2
- [12] Evonne Ng, Donglai Xiang, Hanbyul Joo, and Kristen Grauman. You2me: Inferring body pose in egocentric video via first and second person interactions. *CoRR*, abs/1904.09882, 2019. 2
- [13] Soohwan Park, Hoseok Ryu, Seyoung Lee, Sunmin Lee, and Jehee Lee. Learning predict-and-simulate policies from unorganized human motion data. *ACM Trans. Graph.*, 38(6), Nov. 2019. 3
- [14] Dario Pavlo, Christoph Feichtenhofer, David Grangier, and Michael Auli. 3d human pose estimation in video with temporal convolutions and semi-supervised training. In *Conference on Computer Vision and Pattern Recognition (CVPR)*, Jun. 2019. 2
- [15] Xue Bin Peng, Pieter Abbeel, Sergey Levine, and Michiel van de Panne. Deepmimic: Example-guided deep reinforcement learning of physics-based character skills. *ACM Trans. Graph.*, 37(4):143:1–143:14, 2018. 3, 4
- [16] Xue Bin Peng, Angjoo Kanazawa, Jitendra Malik, Pieter Abbeel, and Sergey Levine. Sfv: Reinforcement learning of physical skills from videos. *ACM Trans. Graph.*, 37(6), Nov. 2018. 3, 4
- [17] Helge Rhodin, Christian Richardt, Dan Casas, Eldar Insafutdinov, Mohammad Shafiei, Hans-Peter Seidel, Bernt Schiele, and Christian Theobalt. Egocap: Egocentric marker-less motion capture with two fisheye cameras. *ACM Trans. Graph.*, 35(6), Nov. 2016. 2
- [18] Grégory Rogez, Philippe Weinzaepfel, and Cordelia Schmid. LCR-Net++: Multi-person 2D and 3D Pose Detection in Natural Images. *IEEE Transactions on Pattern Analysis and Machine Intelligence*, 2019. 2
- [19] John Schulman, Filip Wolski, Prafulla Dhariwal, Alec Radford, and Oleg Klimov. Proximal policy optimization algorithms. 2017. 4
- [20] J. Tan, K. Liu, and G. Turk. Stable proportional-derivative controllers. *IEEE Computer Graphics and Applications*, 31(4):34–44, Jul. 2011. 4
- [21] Denis Tome, Patrick Peluse, Lourdes Agapito, and Hernan Badino. xr-egopose: Egocentric 3d human pose from an hmd camera. In *Proceedings of the IEEE International Conference on Computer Vision (ICCV)*, pages 7728–7738, Oct. 2019. 2
- [22] S. Wang, R. Clark, H. Wen, and N. Trigoni. Deepvo: Towards end-to-end visual odometry with deep recurrent convolutional neural networks. In *IEEE International Conference on Robotics and Automation (ICRA)*, pages 2043–2050, May 2017. 2
- [23] Weipeng Xu, Avishek Chatterjee, Michael Zollhoefer, Helge Rhodin, Pascal Fua, Hans-Peter Seidel, and Christian Theobalt. Mo²Cap²: Real-time mobile 3d motion capture with a cap-mounted fisheye camera. *IEEE Transactions on Visualization and Computer Graphics*, pages 1–1, 2019. 2
- [24] Ye Yuan and Kris Kitani. 3d ego-pose estimation via imitation learning. In *The European Conference on Computer Vision (ECCV)*, Sep. 2018. 2, 3
- [25] Ye Yuan and Kris Kitani. Ego-pose estimation and forecasting as real-time pd control. In *IEEE International Conference on Computer Vision (ICCV)*, pages 10082–10092, Oct. 2019. 2, 3, 4, 6, 7
- [26] Ye Yuan and Kris Kitani. Residual force control for agile human behavior imitation and extended motion synthesis. In *Advances in Neural Information Processing Systems*, 2020. 3